JYX
JYVÄSKYLÄN YLIOPISTO
UNIVERSITY OF JYVÄSKYLÄ

This is a self-archived version of an original article. This version may differ from the original in pagination and typographic details.

Author(s): Heiskanen, Samuli; Geng, Zhuoran; Mastomäki, Jaakko; Maasilta, Ilari J.

Title: Nanofabrication on 2D and 3D Topography via Positive-Tone Direct-Write Laser Lithography

Year: 2020

Version: Accepted version (Final draft)

Copyright: © 2019 WILEY-VCH Verlag GmbH & Co. KGaA

Rights: In Copyright

Rights url: http://rightsstatements.org/page/InC/1.0/?language=en

Please cite the original version:

Heiskanen, S., Geng, Z., Mastomäki, J., & Maasilta, I. J. (2020). Nanofabrication on 2D and 3D Topography via Positive-Tone Direct-Write Laser Lithography. Advanced Engineering Materials, 22(2), Article 1901290. https://doi.org/10.1002/adem.201901290

Nanofabrication on Two- and Three-dimensional Topography via Positive-tone Direct-write Laser Lithography

*Samuli Heiskanen, Zhuoran Geng, Jaakko Mastomäki, Ilari J. Maasilta**

Samuli Heiskanen, Zhuoran Geng, Jaakko Mastomäki, Prof. Ilari J. Maasilta
Nanoscience Center, Department of Physics, University of Jyvaskyla, P. O. Box 35, FIN-40014 Jyväskylä, Finland
maasilta@jyu.fi

Keywords: nanofabrication, direct laser writing, two-photon absorption, positive-tone resist, lift-off

Direct laser writing (DLW) lithography using two-photon absorption is a powerful technique mostly used for fabrication of complex structures in micro- and nanoscale, by photopolymerizing a negative-tone resist. In contrast, in this study it is demonstrated that DLW is also well suited for fabricating nano- to microscale metallic structures using lift-off and a positive-tone photoresist. It is shown first that versatile, fast and large area fabrication is possible on flat two-dimensional insulating substrates, and an expression for how the line width varies with the scanning speed is derived, with excellent agreement with the experiments. Even more interestingly, a unique application for the DLW lift-off process is demonstrated, by fabricating sub-micron scale metallic wiring on uneven substrates with sloping elevation changes as high as 20 μm. Such fabrication is practically impossible with more standard lithographic techniques.

I. INTRODUCTION

Three-dimensional, direct laser writing (DLW) lithography based on two-photon absorption is a fairly recent and powerful technique used for three-dimensional writing of nano- and microscale structures into photoresists. [1–3] Some of the main application areas demonstrated are photonics,[4, 5] micro-optics,[6, 7] mechanical metamaterials,[8, 9] microfluidics,[10, 11] biomimetics,[12, 13] and micro and cell biology,[14–16] to name a few.

In most of these applications, the goal of the fabrication is the direct patterning of complex shapes, and as such, negative-tone photoresists, where exposed areas form the final structure, are often preferred and heavily used. Moreover, typically the highest resolution resists are liquids, allowing only negative-tone operation.

On the other hand, in traditional top-down nano- and microfabrication such as planar 2D UV photolithography and electron beam lithography, positive-tone solid-state resists are very commonly used as a mask in nano- and microscale electrical device fabrication, where the exposed regions can be removed in a development step. This is highly useful where small features are deposited onto or etched into the substrate, as only the small feature areas (lines, dots, etc.) need to be exposed.

In contrast, in the field of direct-write two-photon absorption (TPA) microfabrication, positive-tone solid-state resists have not been so widely employed. For 3D structuring, combining positive-tone resists with electrodeposition of metallic structures without electrical contacts and lift-off was demonstrated for photonic [17] and mechanical metamaterials,[18] magnetic microrobots[19] and magnetic nanostructures,[20] with the smallest feature size in the metal around 400 - 500 nm. In addition, 3D 4 μm $\times$ 4 μm microchannel structures [21] and micrometer scale molds [22] have also been demonstrated via positive-tone resists and TPA writing. In addition, a recent study [23] also pointed out the relevance of TPA direct writing in fabricating purely 2D, large area metallic nanostructures (feature sizes above 400 nm) designed for plasmonic applications, using a positive-tone resist and lift-off.

In this paper, our focus is twofold: First we demonstrate the capabilities of the TPA writing for flat surfaces in the fabrication of long and narrow metal wiring and wire meshes using a positive-tone resist and lift-off, and discuss its strengths in comparison with more traditional lithographic techniques. Second, and perhaps more importantly, we also demonstrate the fabrication and electrical measurement of sub-micron conducting wiring on uneven, three-dimensional topography using a positive-tone photoresist and DLW two-photon absorption fabrication. Especially this second application offers unique opportunities, as such fabrication is not available with traditional electron beam, ion beam or photolithography. Inkjet printing could be used to pattern some materials onto uneven surfaces, but the resolution available with that technique is typically about an order of magnitude inferior, and it is limited by the available metal nanoparticle pastes.

It is also possible, alternatively, to use DLW to write metallic structures using photore-

duction, even in 3D. [24, 25] Although those techniques are promising, the method presented here has the benefit that it relies on the established photoresists and evaporation techniques, known to produce high quality pure materials with low roughness, important for advanced devices such as tunnel junctions, for example. In addition, the whole palette of metals is available, whereas the range of materials (Ag, Au and Cu) and their quality (often metal-polymer composites) produced by the DLW photoreduction technique is limited by the chemistry involved. [24, 25]

The paper is organized as follows: We first systematically investigate the quantitative characteristics of applying our DLW nanofabrication tool (Photonic Professional by Nanoscribe GmbH) to a positive-tone solid-state resist which has not been reported before for TPA lithography (AR-P 3120 photoresist by Allresist GmbH). We use both the common immersion objective method, Figure 1a, which can only be used with transparent substrates, and the air-gap objective method, Figure1 b – c, suitable also for opaque substrate materials. Section II A first describes the writing tests on the resist using an immersion objective, whereas in Section II B we compare similar results obtained with an air-gap objective. In section III, we demonstrate some examples of a full fabrication process of metallic wiring structures, using lift-off on flat surfaces, down to 330 nm wire width and 650 nm pitch. Finally, in section IV, we demonstrate the fabrication of metallic wiring on complex, engineered three-dimensional topography.

II. RESOLUTION AND SPEED OF TWO-DIMENSIONAL PATTERNING USING A POSITIVE-TONE RESIST

A. Resist tests on glass substrates using an immersion objective

The exposed volume in the positive-tone resist will be removed after the development, leaving openings to the resist, in contrast to negative-tone resists, where the exposed volume is polymerized and thus directly forms the corresponding voxel shape. This gives us a way to measure the lateral resolution of the voxel under scanning electron microscopy (SEM). First, we study the lateral resolution of both stationary spots and continuously scanned lines as a function of the laser output power, the spot exposure time or the scan speed.

Using the immersion oil method (details in section VI), we first systematically exposed

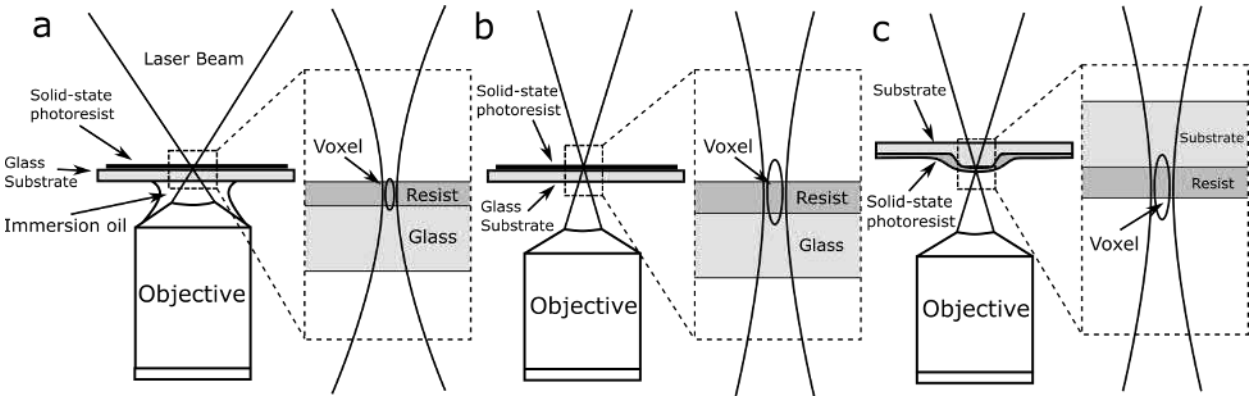

Figure 1. Different exposure methods used. (a) Immersion objective method, widely used in TPA lithography process. An inverted high numerical aperture (NA) objective is dipped into immersion oil, with the refraction index matched to the glass substrate used. A laser beam is tightly focused around the interface between the photoresist and the front surface of the glass substrate, where the TPA process forms the voxel. (b) Air-gap objective method through a glass substrate. An inverted objective is not in contact with the substrate, but has an air-gap. A laser beam is tightly focused as before. (c) Air-gap objective method for writing on uneven topography. An inverted objective is not in contact with the substrate, but has an air-gap. The laser beam focus travels in z-direction, following the existing topography on the front surface, where the TPA process forms the voxel.

our sample at single stationary locations, with varying laser power (ranging from 0.2 mW to 8 mW) and exposure time (ranging from 0.8 ms to 1 s), see Figure 2d. The laser focus was kept at the resist to air interface. The lateral diameters of the exposed spots were measured with an SEM (eLiNE, Raith GmbH, manual fitting), and plotted as a function of exposure time t with different laser output powers, as shown in Figure 2a, and as a function of laser output power P with different exposure times, as shown in Figure 2b. In both figures, theoretical fits to a function $A\sqrt{\ln(BP^2t)}$ (with A and B the fitting parameters) are also shown, with excellent agreement. This non-linear dependence is based on known TPA theory, [26, 27] and agrees with studies on negative-tone [26, 28, 29] and positive-tone [30] resists reported by other groups. We stress that we only plot exposures that resulted in well behaving round spots, as exemplified in Figure 2d. Odd-shaped spots were typically generated when the resist was underexposed and thus more susceptible to external interference such as vibrations and acoustic noise.

Moreover, we found that the voxel diameter dependence on the laser power P and the exposure time t can be combined into a collective exposure parameter P^2t, where the square of the laser power P^2 is multiplied by the exposure time t, see Figure 2c. This dependence is in agreement with the non-linear absorption rate of the second order photons in the TPA process, as seen before,[27] and indicates that it is this collective exposure parameter (proportional to an effective dose) that needs to be tuned, based on the requirements for the resolution in the AR-P 3120 positive-tone resist lithography. Note that for one-photon absorption, the effective dose would be proportional to Pt instead.

We performed another experiment by continuously exposing the sample with different stage scanning speeds, ranging from 10 μm s^{-1} to 400 μm s^{-1}, using different laser output powers (ranging from 2 mW to 6 mW). The line width was again measured with the SEM (Figure 3d), and in Figure 3a we plot the measured width as a function of the stage scanning speed, with different laser output powers. From Figure 3a we see that the line width has clearly a non-linear dependence on the scanning speed, as can be seen from the fitting functions. These fits we obtained using a theory for the line width w, derived in the Supporting Information, assuming linear motion of the laser spot with speed v:

$$w = \omega_0\sqrt{\ln\left(\frac{\sigma_2 I_0^2}{C}\frac{\sqrt{\pi}}{2}\frac{\omega_0}{v}\right)}, \tag{1}$$

where ω_0 is the beam waist at the focal plane, σ_2 the effective two-photon cross section, I_0

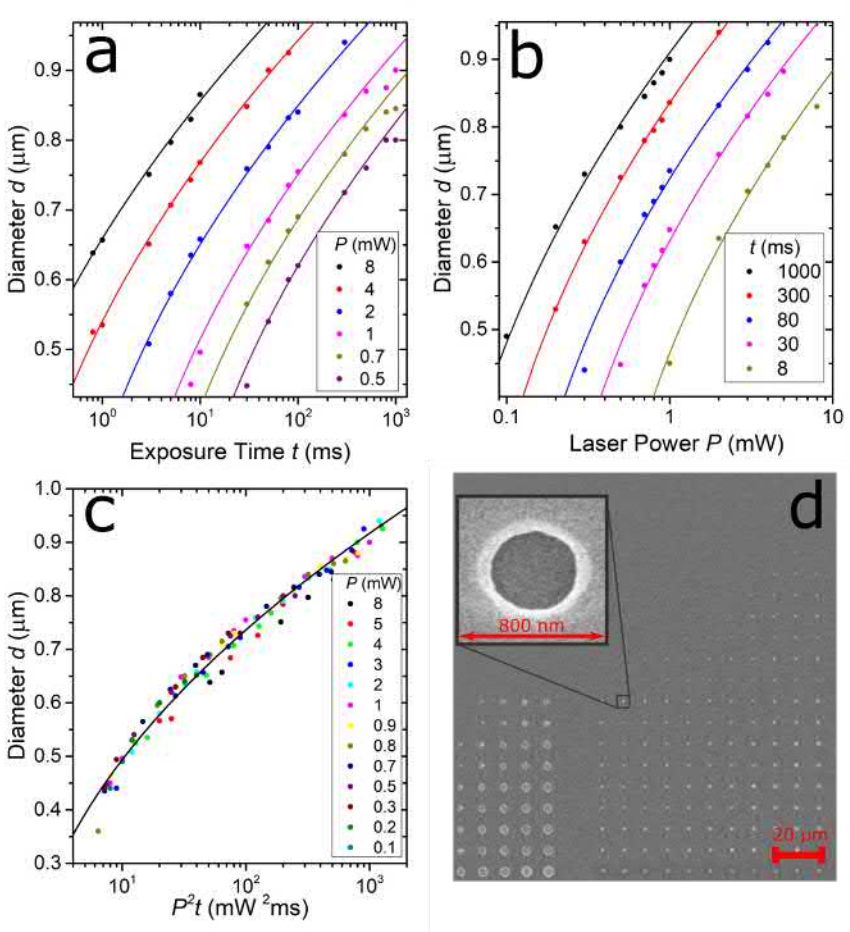

Figure 2. Point tests with the immersion oil method. (a) Diameter of the exposed spots as function of exposure time, with different laser output powers. The solid points are the SEM measured data, the solid lines are theoretical fits. (b) Diameter of the exposed spot as function of laser output power with different exposure times. The solid points are the SEM measured data, the solid lines are theoretical fits. (c) Diameter of the exposed spot as a function of the collective exposure output P^2t. The solid points are the SEM measured data, the solid line is a theoretical fit. All the fits use a two-parameter function $A\sqrt{\ln(BP^2t)}$, with values $A = 360$ nm, $B = 6.55 \times 10^8$ $\mathrm{W}^{-2}\mathrm{s}^{-1}$ for the fit to all data in (c). (d) SEM image of a grid of point exposures with different exposure parameters, with the inset showing an example of an exposed spot after development.

is the time-averaged laser beam photon flux intensity at the beam center (photons/area/s), and $C = \ln[\rho_0/(\rho_0 - \rho_{th})]$ a resist dependent material parameter [26, 27], with ρ_0 the initiator density and ρ_{th} the threshold density for radicals to initiate reaction in the resist. In the experiment, the parameter controlling I_0 is the output power of the laser P, as there is a direct proportionality between the two [26, 27].

Comparing to the spot exposure experiment, Equation (1) predicts that the exposure parameter controlling the line width in scanning mode is P^2/v instead of P^2t. We can check this by plotting all line width data as a function of P^2/v, as shown in Figure 3c. Again, we obtain great agreement between the experiment and the theory, except at the highest P^2/v values, where possibly the density of radicals saturates and diffusion rate starts increasing.

Based on Equation (1), we see that for a fixed target line width w, if one wants to increase writing speed, the power does not need to be increased linearly, as would be the case for one-photon absorption, but only as a square root. Figure 3b shows this fact for our experimental conditions, where we plot the quadratic scanning speed increase with the increased laser output power, for three different line widths, based on the fits of Figure 3a. The possibility to increase the scanning speed quadratically with the laser output power enables ultrafast DLW for a large scale 2D fabrication. As we see from Figure 3b, one could use writing speeds of $\sim$ 6 mm s^{-1} for a 400 nm line for this resist with a realistic output power of 10 mW. Unfortunately, in this study, we were limited by the accuracy of our motorized stage, and could not test the ultrafast DLW mode at speeds above mm s^{-1}. Setups using galvo mirrors (commercially available), can reach up to 20 mm s^{-1} scanning speeds,[31] and fast TPA writing with such a setup and a different resist (AZ MiR 701) was demonstrated before [23]. Moreover, the non-linear relation between the scan speed and the line width can also be utilized as a velocity-dependent "shutter mechanism" for DLW without using physical shutters, as reported before for the negative SU-8 resist [29].

Note that smaller diameters and line widths of the order of 100 nm have been reported in the literature for DLW writing into a positive-tone resist [30], using a much thinner resist layer of $\sim$ 150 nm. The thin resist allows one to shift the focus plane in such a way to use only the tip of the voxel, to gain in resolution. However, this type of tuning was not considered in this study, as the resist profile generated in such a manner [30] is not suitable for lift-off and transfer of the pattern to metallic structures.

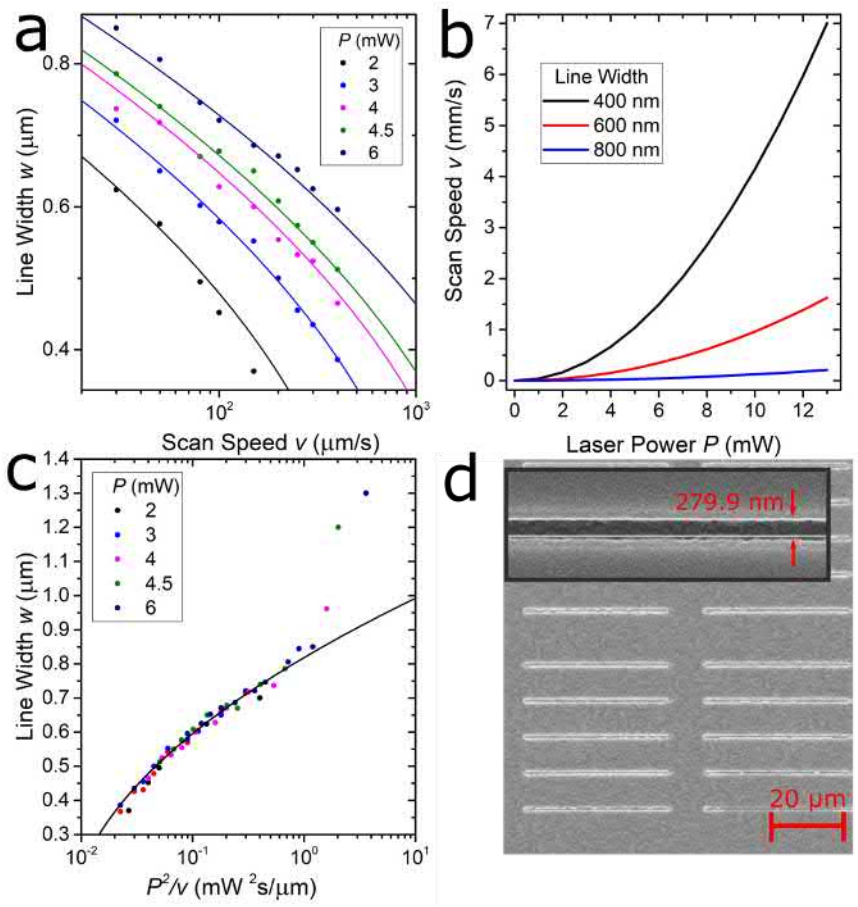

Figure 3. Line tests with the immersion oil method. (a) Measured line width as function of the stage scan speed, with different laser output powers. The solid points are the measured data, and the lines are two-parameter fits to the theory of Equation (1). (b) Simulation of the stage scan speed as a function of laser output power for different desired line widths, based on the measured data. (c) Measured line width as a function of the collective exposure parameter P^2/v. The solid points are the measured data, the solid line is a two parameter fit based on the theory of Equation (1) $w = A\sqrt{\ln(BP^2/v)}$, with $A = 370$ nm, $B = 133.4$ m W^{-2}s^{-1}. (d) SEM image of a grid of line exposures with varying exposure parameters. The inset is a zoomed-in SEM image of an exposed line after development.

B. Resist tests on glass substrates using an air-gap objective

Direct laser writing can be also performed with an air-gap objective, which provides a more versatile alternative to an immersion oil objective, as it is not in contact with the substrate. This makes it possible for example to expose features on the front side of opaque substrates, and particularly on an already existing larger surface topography, an option we will focus on in Section IV. However, for comparison with the results obtained above with the immersion oil objective, we first study the characteristics of exposing the same AR-P 3120 positive-tone resist through glass substrates with the air-gap objective (NA= 0.75, magnification 63 x , Zeiss GmbH), see Figure 1b. An obvious drawback of such an air gap objective is its lower resolution. However, if 1 – 2 micron scale features are wanted, the writing speed can be faster compared to the immersion oil method.

As in section II A, the resolution of the air-gap method was studied by measuring the diameter of single spots exposed by varying the laser power P and the exposure time t (Figure 4a), and by measuring the line widths by varying the laser power P and the stage scanning speed v (Figure 4b), with the laser focused at the surface of a 500 nm thick resist. The smallest spots and lines have dimensions $\sim$ 400 nm, but they do not go completely through the resist. The optimal points have a larger 600 nm - 800 nm diameter. As before for the immersion oil method, the theories for the spot diameter [26, 27, 30] and the line width, Equation (1), fit very well to most of the data, when plotted as a function of the correct combined effective dose parameters (P^2t for spots P^2/v for lines), as evident in Figs 4c and d. Only at the highest effective dose ranges do the diameters and widths increase beyond what is expected from the theory. This effect, which is an abrupt change in the case of stationary spots, was observed to be caused by the collapse of the overhanging edges, as the exposed resist profile has an undercut at high doses. From Figure 4b we also see that we managed to use high speeds of 2 mm s^{-1} to write lines of width below 500 nm.

Another interesting aspect is the length of a voxel at different working parameters. This was studied by moving the laser focus vertically so that the length of a voxel can be determined from the end points where the very "tail" of a voxel still exposes the resist. The plot of the voxel length as a function of P^2t is shown in Figure 5. The results indicate that voxels are rather tall ($\approx$ 2 µm) even with the lowest doses. However, an elongated voxel is a benefit for 2D patterning: A thicker resist can be exposed with a single pass line, with an

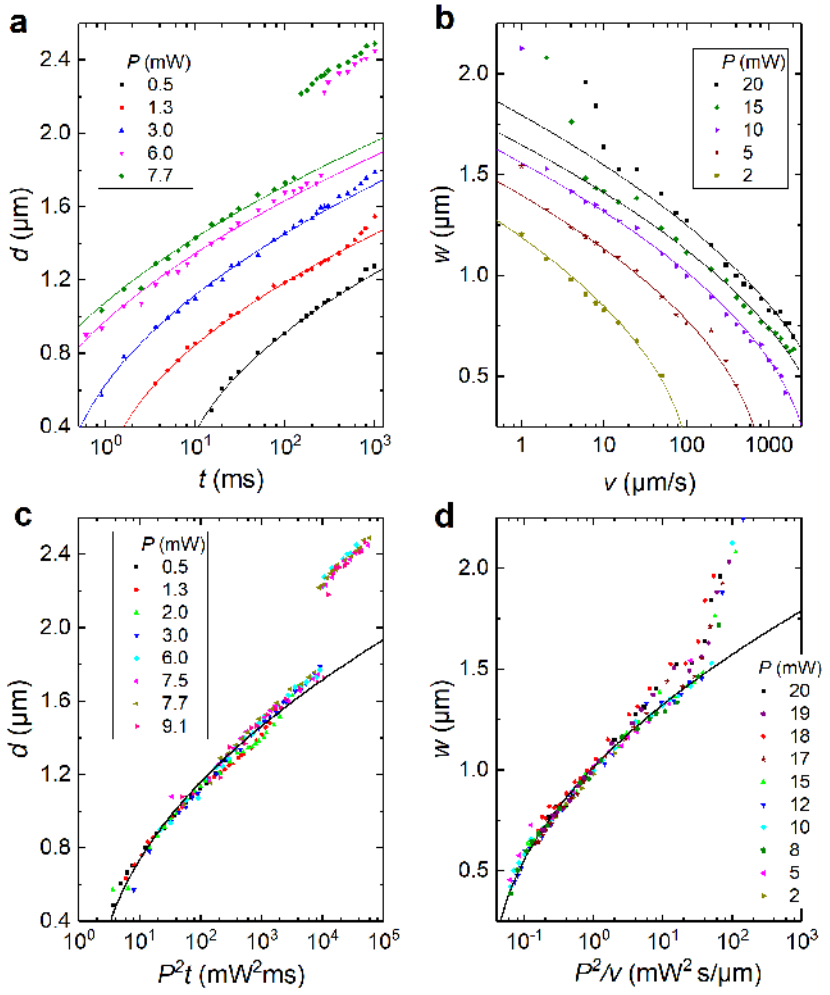

Figure 4. Point and line tests with the air-gap method. (a) Diameter of single spots exposed with the air gap objective, as a function of the exposure time t and the laser power P (points). The lines are the best fits to functions $A\sqrt{\ln(BP^2t)}$. (b) Width of the exposed lines as function of the stage scanning speed with different laser output powers. The lines are two-parameter fits to Equation (1). (c) Diameter of the exposed spots as a function of the combined exposure parameter P^2t. The points are the SEM measured data, the solid line is a two-parameter fit to $A\sqrt{\ln(BP^2t)}$ with $A = 590$ nm, $B = 4.78 \times 10^8$ W^{-2}s^{-1}. (d) Measured line widths as a function of the combined exposure parameter P^2/v. The points are the measured data, the solid line is a two parameter fit based on the theory of Equation (1), $w = A\sqrt{\ln(BP^2/v)}$, with $A = 560$ nm, $B = 26.9$ m W^{-2}s^{-1}. The discrepancy between the theory and experiment at high effective doses is due to the collapse of the undercut profile of the resist, and those points were excluded from the fits.

aspect ratio of roughly 5:1. To expose resists thicker than $\sim 1\mu$m, several passes at different vertical focal points can easily be used. Also, we point out that the undercut profile can likely be tuned by choosing an appropriate ratio between the resist thickness and the voxel length, and by the placement of the focal plane. Undercut control is of course quite critical for a successful lift-off processing, one of the major ways of using positive-tone resists.

III. LARGE-SCALE FABRICATION OF SUB-MICRON METALLIC WIRING ON FLAT GLASS SUBSTRATES

With the above exposure knowledge, we have designed and fabricated metallized prototype samples, using the immersion oil DLW technique. It is quite important to demonstrate a complete fabrication sequence for devices, not just resist exposure tests, including metal evaporation and lift-off. We are aware of only one previous report [23] that studied TPA DLW writing with positive-tone resist in such a manner. One of the possible applications with this technique is the fabrication of sub-micron cm-long conducting wires and wire grids on transparent substrates, for electro-optical experiments. Such samples would be much harder, if not impossible, to fabricate with more standard techniques such as electron-beam lithography, due to difficulties with charging and stitching of the write fields.

The sample, shown schematically in Figure 6a, contains several sets of 2 cm long, continuous and electrically conducting silver lines on a transparent glass substrate, with design line widths 450, 600 and 800 nm. For the narrowest line sets we thus have an ultrahigh aspect ratio of width to length over $1 : 40,000$. The sample also contains two 3 mm $\times$ 3 mm square mesh structures, which consist of hundreds of either 450 nm or 600 nm wide, 3 mm long crossing silver lines (Figure 6b). This sample thus demonstrates the advantages of TPA DLW for high resolution, stitching free, charging free, fast scanning speed, large scale, versatile nanofabrication.

The sample is fabricated on a 170 μm thick glass substrate using a 500 nm thick layer of AR-P 3120 photoresist, spin coated and developed as described in section VI. The line width was controlled by a combination of the laser power and scanning speed used, with a 2 mW, 2.5 mW, and 4 mW laser power, and 300 μm s^{-1}, 180 μm s^{-1}, and 50 μm s^{-1} stage scanning speed used during the exposure for the 450 nm, 600 nm, and 800 nm line widths, respectively. Note that the scanning was performed with a motorized stage instead of the

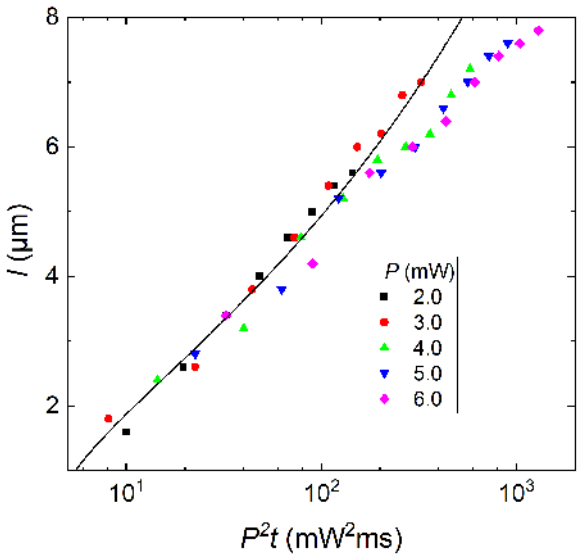

Figure 5. Voxel length l vs. P^2t for a few laser powers, with a fitting function $l = A\sqrt{\sqrt{BP^2t} - 1}$ based on known TPA theory [26, 27], with $A = 2.48$ μm, $B = 2.47 \times 10^8$ W^{-2}s^{-1}. The voxel length is determined by exposing points at different laser focus heights with respect to the surface of the resist, and calculating the distance between the first and the last exposed point. The discrepancy between the theory and experiment at high effective doses is due to the collapse of the undercut profile of the resist, and those points were excluded from the fits.

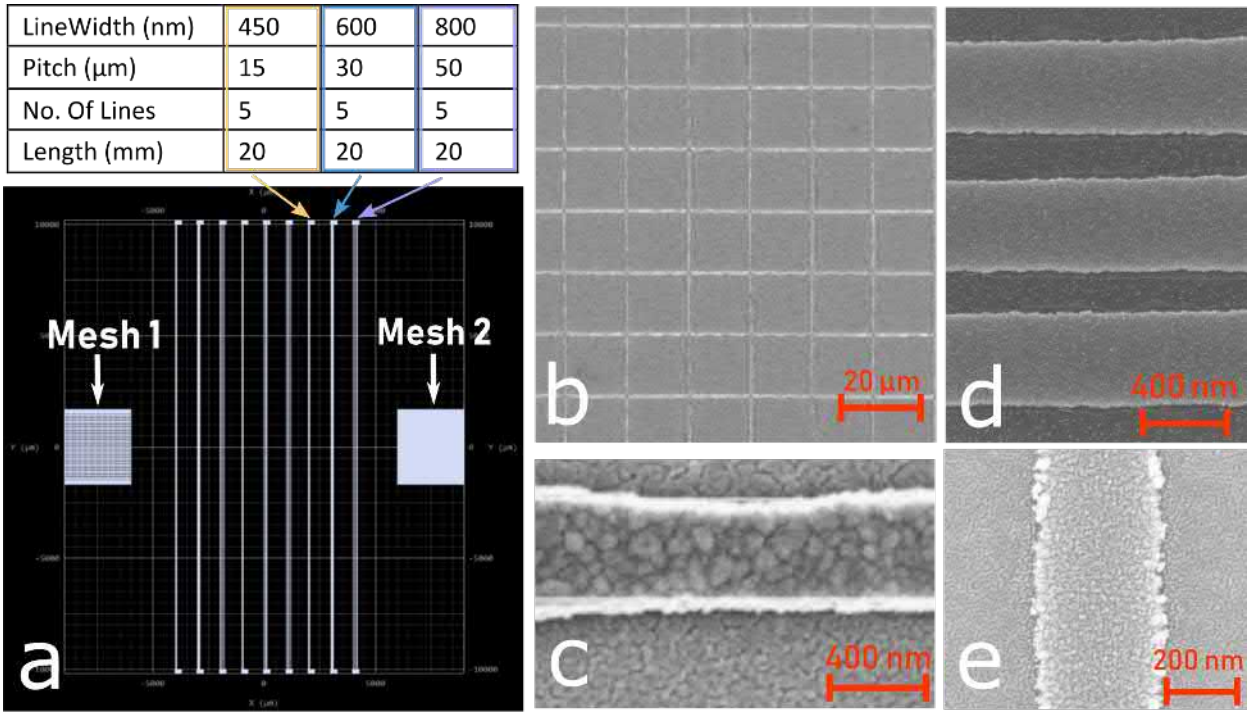

Figure 6. Large-scale wire fabrication on a flat substrate. (a) Design of the 2D test sample. Groups of 20 mm long silver lines, with each group consisting of three sets of lines with three different line widths (450 nm, 600 nm, 800 nm), are located at the central region of the sample. In each line set, five identical lines are connected by a contact pad at each end. Two 3 mm $\times$ 3 mm square mesh structures are located to the left (Mesh 1) and right (Mesh 2) of the wires, with Mesh 1 (Mesh 2) consisting of 122 (402) 450 nm (600 nm) wide, 3 mm long sets of silver lines of pitch 50 μm (15 μm). (b) SEM image of a part of the 450 nm meshed silver grid. (c) Zoomed-in SEM image of a section of 450 nm wide, 20 mm long silver line. (d) SEM image of 450 nm wide titanium lines with a 200 nm distance between them. (e) An SEM image of a 330 nm wide titanium line.

piezoelectric scanner, to allow for scanning lengths beyond the scan range of the piezostage, limited to 300 μm. After development, the exposed glass surfaces were cleaned by a 40 mTorr, 40 W, 50 sccm oxygen plasma cleaning process in a reactive ion etcher, followed by an ultra-high vacuum (1×10^{-8} mbar) e-beam evaporation of a 200 nm thick silver film. After the evaporation, lift-off was done with hot AR 300-76 remover (Allresist GmbH) with a 2 sec sonication.

Figure 6b shows a representative SEM image of a part of the 450 nm silver mesh, and Figure 6c presents an example of a higher magnification SEM image of a long 450 nm silver line. As contact pads were also fabricated, we were also able to perform resistivity measurements on the structures, demonstrating the continuity of lines across such long lengths.

We also fabricated samples to find the resolution limits for this technique. For these samples the same AR-P 3120 resist was used, but the thickness was lowered to 450 nm and the piezoelectric scanner was used for more accurate control of the scanning speed. Instead of silver, we used titanium for the metallization to improve adhesion. To find the highest possible pitch, we fabricated a sample with varying pitch, laser power and focal height. The scanning speed was kept at 20 μm s^{-1} based on the dose tests. With a 3 mW laser power and the laser focus at 400 nm below the resist surface we achieved 450 nm lines with a 200 nm distance between them (Figure 6d). Similarly, we found the narrowest possible line, but now instead of the pitch we also varied the scanning speed. The narrowest line was 330 nm wide (Figure 6e), drawn with a 2.5 mW laser power and a 50 μm s^{-1} scanning speed.

IV. WIRE FABRICATION ON THREE-DIMENSIONAL TOPOGRAPHY

Next, we demonstrate an even more promising application of 2D TPA DLW lithography: fabrication of metallic wiring on uneven surface topography. This application is very useful, as such a fabrication is extremely challenging with more standard photo- or e-beam lithographic techniques which operate on a flat focal plane. The uneven writing surface is not a problem with TPA DLW, because the required height changes for the focal plane can easily be included in the wire design, as the sample stage can be moved in all coordinate directions. The technique also allows trivially the use of nonconducting substrate materials, in contrast to e-beam lithography. For this application, the air-gap objective is the only

choice as the exposure needs to be done from the side of the 3D topographic structures, and not through the substrate, schematically shown in Figure 1c. This is because of limitations of the working distance for through-substrate writing. Also, if the laser would have to travel through multiple interfaces and the 3D structures, the laser intensity and resolution would be reduced. Writing through the substrate would also limit the usable substrate materials.

Wire fabrication on 3D topography was tested by first fabricating tall structures using the same DLW system. In this case the structures were fairly simple cuboidal structures of height 20 μm, shown in Figures 7a and b, with ramps on the sides so that wiring from the substrate surface can be routed onto the cuboid. The cuboid structures were fabricated using the DiLL (Dip in Laser Lithography) method, in which an objective (NA = 1.3, 100 x) is dipped in a liquid negative-tone photoresist (IP-Dip, Nanoscribe GmbH) for the exposure and photo-polymerization. Transparent sapphire substrates were used to reduce reflections at the interface between the resist and the substrate.

After their fabrication, the cuboid structures need to be coated with the positive-tone AR-P resist for the wire fabrication (details in Section VI). Straightforward spin coating cannot be used due to the large 20 µm height of the structures, instead, direct spray coating [32] could be used. However, this method was not available to us, so we had to make modifications to the cuboid structure itself, to still allow for spin coating. First, walls had to be added to the outer rim of the cuboid, to create a sort of a bowl for the resist to stay in during spin coating (Figure 7b. Second, the structures were made much wider ($\sim$ 60 μm $\times$ 60 μm), otherwise the proximity of the walls to the metal wiring would make the lift-off process unnecessarily hard. The walls are sloped on the inside to reduce their horizontal surface area. This smaller surface area reduced the amount of resist that adheres to the walls in the lift-off process.

Before doing the lithography for the wiring, most 3D-structures were conformally coated with a 50 nm layer of aluminum oxide using atomic layer deposition (ALD) [33]. This was done to make the structures mechanically stronger for the lift-off, although successful lift-off was also shown to be possible for non-coated, pure IP-Dip polymer structures. After the ALD coating, the structures were spin coated with four nominally 800 nm thick layers (1500 RPM and time 90 s) of the AR-P 3120 resist to get good coverage also on top of the structures.

Then the samples were exposed with DLW for the wiring with a line pattern that follows

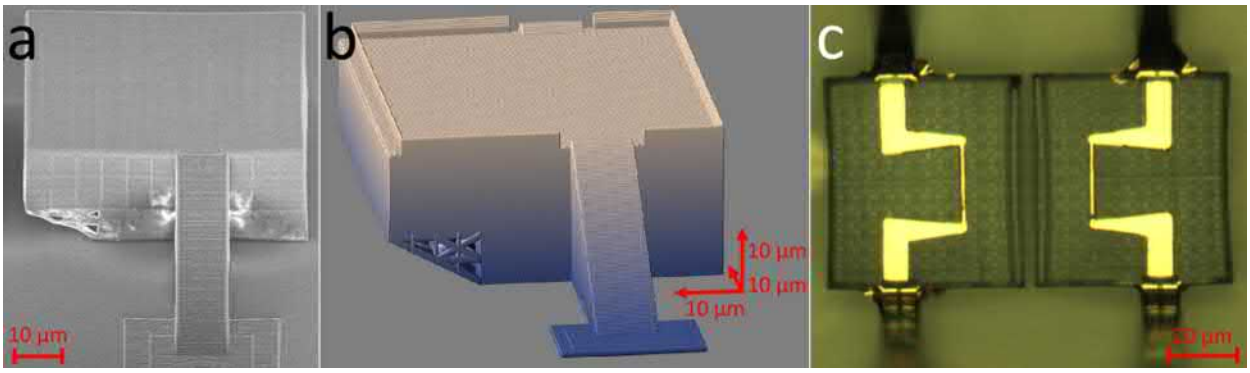

Figure 7. Wire fabrication on 3D topography. (a) SEM micrograph of a 3D cuboid structure without side walls, also fabricated with DLW, from a side angle view. The height of the structure is about 20 µm. (b) Design of the modified 3D-cuboid structure with walls surrounding the elevated platform. The width of the platform is 60 µm. (c) Top-view optical micrograph of finished samples with deposited gold wiring traveling from the substrate to the platform. The width of the thinnest section of the wiring is about 1 µm.

the ramp and platform topography of the underlying cuboid structure in 3D space, with alignment performed with the integrated optical microscope before the exposure. A writing speed 20 µm s^{-1} was used, and the width of the lines was determined by changing the laser power between 10 mW and 20 mW, producing a smallest line width $\sim$ 800 nm. With faster speeds or lower power values the resist was not fully exposed. At the base of the cuboid, several passes with varying focal points in z-direction were used to fully expose the somewhat thicker resist that accumulated in those regions.

After the development, the samples were coated with a $\sim$ 70 nm gold layer, with a thinner $\sim$ 20 nm titanium adhesion layer underneath, by electron beam evaporation in ultra-high vacuum. The evaporation had to be done from multiple angles from the sides of the ramps, to get good film coverage also on the ramps (Section VI), as they contained small $\sim$ 100 nm vertical steps, as can be seen in Figure 7 a. A finished sample with gold wiring routed from the substrate surface onto the cuboid platform using the ramps is shown in Figure 7c. As the figure shows, we have successfully demonstrated metal wire fabrication on 20 μm tall 3D structures, with the wiring climbing the structure from the substrate surface, using DLW and lift-off with a positive-tone resist. The continuity of the wiring was also demonstrated with electrical measurements, with the observed room temperature resistance values typically around 35 - 40 Ω. For one sample, we also characterized the temperature dependence of the resistivity, showing a standard metallic behavior and an RRR of $\sim$ 2.8.

V. CONCLUSIONS

Our results clearly demonstrate the capabilities of DLW using two-photon absorption also for 2D lithography with lift-off, with metallic lines down to 450 nm width fabricated on vary large areas, up to 2 cm. On smaller areas, 650 nm pitch and 330 nm line width were also demonstrated. As 2D lithography and lift-off are very common and established techniques in general, we should critically evaluate the strengths and weaknesses of using the TPA DLW technique for this purpose. The fact that the writing is maskless gives it versatility and suitability for research problems and prototyping, as opposed to standard photolithography that uses masks. Direct laser writing, on the other hand, can be done in 2D with one-photon absorption, if UV lasers are used. A typical writing speed with the highest resolution (nominally around 300 nm) of such a laser lithography tool is of the order

of mm s^{-1}, in other words, the resolution and speed are similar to what was demonstrated here. The main difference between one-photon and two-photon absorption comes with how the line width scales with intensity, Equation (1). It means that if the intensity of the laser can be increased, the writing speed increase is quadratic for two-photon as opposed to linear in one-photon absorption, favoring TPA eventually.

Even though the lift-off worked for the processing described here, one can also envision simple improvements that would enhance the undercut profile and thus help the lift-off. One could implement the well known technique, where two layers of different resists are used, with the more sensitive layer underneath. In addition, the TPA DLW technique uniquely allows for writing just one layer of resist at two different heights with different exposure parameters, which can be used to tune the undercut profile.

Even more promising, however, is the possibility we demonstrated here that 2D lithography is performed on uneven, non-flat topography. This seems to be the strong point of doing 2D lithography with an inherently 3D lithography system. We showed the feasibility of fabricating sub-micron scale metallic wires on a three-dimensional structure with an elevation change as high as 20 μm, on a complex structure, using a positive-tone resist and lift-off. Such fabrication is extremely challenging, if not impossible, with more standard techniques that have to rely on the flatness of the substrate.

VI. EXPERIMENTAL SECTION

Two-photon lithography tool The DLW nanofabrication tool used (Nanoscribe Photonic Professional) is based on a 80 MHz repetition rate pulsed fiber laser with a near infrared wavelength (780 nm), with maximum laser power of 90 mW. A three axis piezo-electrical stage is used for accurate motion of the substrate of distances below 300 μm, and a motorized stage is used for larger area movements.

Immersion objective method In the immersion objective method, a transparent glass substrate with 170 μm thickness was mounted on the piezo-electrical stage with the resist side facing up, and an inverted microscope objective with 100× magnification and 1.4 numerical aperture (NA) was dipped into the immersion oil on the backside of the substrate as shown in Figure 1a. Instead of using the conventional liquid negative-tone resist, we used a spin coated, solid, positive-tone UV photoresist AR-P 3120, consisting of novolac resin and

naphthoquinone diazide. The thickness of the resist was controlled by the spin speed and a short pre-exposure baking immediately followed after the spin. In our case, a 500 nm thick resist was spun with 5000 RPM for 60 sec, followed by a bake for 1 min at 100 °C. After the laser exposure, the sample was first developed in a 1 : 1 mixture of AR 300-47 and deionized water for 1 min, then rinsed for 2 min in pure deionized water, and finally blow-dried with nitrogen gas.

Air-gap objective method, writing through glass In the air-gap objective method, an objective (Zeiss GmbH) with NA= 0.75 and magnification 63 x was used, not in contact with the substrate. A transparent glass substrate with 170 μm thickness was mounted on the piezo-electrical stage with the resist side facing up. The same spin-coated, solid, positive-tone UV photoresist AR-P 3120 was used (500 nm thickness), spun with 5000 RPM for 60 sec, followed by a bake for 1 min at 100 °C, and developed in a 1 : 1 mixture of AR 300-47 and deionized water for 1 min, then rinsed for 2 min in pure deionized water, and blow-dried with nitrogen gas.

Air-gap objective method, wire deposition on the 3D topography The 3D structures were spin coated with four 800 nm thick layers (1500 RPM and time 90 s) of the AR-P 3120 resist, which was baked at 100°C for 30 s between layers and for 1 min after the last layer. After the exposure and development (1:1 solution of AR 300-47 and deionized water for 1 min), the samples were coated with a $\sim$ 70 nm gold layer, with a thinner $\sim$ 20 nm titanium adhesion layer underneath, by electron beam evaporation in ultra-high vacuum. The evaporation was done from six different angles from both sides of the structure, first Ti, then Au, in a sequence shown in Table I below. The lift-off was done with heated and sprayed AR 300-76 remover.

Electrical characterization of the samples The metalized wire samples of Section III were electrically characterized by measuring their resistance with a Keithley 2450 SourceMeter at room temperature. The resistance of the wiring on the three-dimensional topography in Section IV was measured with a multimeter, and in the case of the temperature dependence, with a Stanford SR830 lock-in amplifier at a frequency of $\sim$ 15 Hz.

Supporting Information

Supporting Information is available from the Wiley Online Library or from the author.

Acknowledgements

This study was supported by the Academy of Finland project number 298667.

[1] H.-B. Sun, S. Matsuo, H. Misawa. *Appl. Phys. Lett.* **1999**, *74*, 786.

[2] S. Kawata, H.-B. Sun, T. Tanaka, K. Takada. *Nature (London)* **2001**, *412* 697.

[3] M. Deubel, G. von Freymann, M. Wegener, S. Pereira, K. Busch, C. M. Soukoulis. *Nat. Mater.* **2004**, *3* 444.

[4] T. Ergin, N. Stenger, P. Brenner, J. B. Pendry, M. Wegener. *Science* **2010**, *328*, 337.

[5] J. B. Reeves, R. K. Jayne, T. J. Stark, L. K. Barrett, A. E. White, D. J. Bishop. *Nano Lett.* **2018**, *18*, 2802.

[6] S. Thiele, K. Arzenbacher, T. Gissibl, H. Giessen, A. M. Herkommer. *Sci. Adv.* **2017**, *3*, e1602655.

[7] E. Johlin, S. A. Mann, S. Kasture, A. F. Koenderink, E. C. Garnett. *Nat. Commun.* **2018**, *9* 4742.

[8] T. Bückmann, M. Thiel, M. Kadic, R. Schittny, M. Wegener. *Nat. Commun.* **2014**, *5* 4130.

[9] L. R. Meza, A. J. Zelhofer, N. Clarke, A. J. Mateos, D. M. Kochmann, J. R. Greer. *Proc. Nat. Acad. Sci.* **2015**, *112*, 11502.

[10] M. H. Olsen, G. M. Hjortø, M. Hansen, Ö. Met, I. M. Svane, N. B. Larsen. *Lab Chip* **2013**, *13* 4800.

[11] Y. Lin, C. Gao, D. Gritsenko, R. Zhou, J. Xu. *Microfluid. Nanofluid.* **2018**, *22*, 97.

[12] M. Röhrig, M. Thiel, M. Worgull, H. Hölscher. *Small* **2012**, *8*, 3009.

[13] X. Liu, H. Gu, M. Wang, X. Du, B. Gao, A. Elbaz, L. Sun, J. Liao, P. Xiao, Z. Gu. *Adv. Mater.* **2018**, *30*, 1800103.

[14] F. Klein, T. Striebel, J. Fischer, Z. Jiang, C. M. Franz, G. von Freymann, M. Wegener, M. Bastmeyer. *Adv. Mater.* **2010**, *22*, 868.

[15] D. Nishiguchi, I. S. Aranson, A. Snezhko, A. Sokolov. *Nat. Commun.* **2018**, *9* 4486.

[16] A. Marino, C. Filippeschi, V. Mattoli, B. Mazzolai, G. Ciofani. *Nanoscale* **2015**, *7* 2841.

[17] J. K. Gansel, M. Thiel, M. S. Rill, M. Decker, K. Bade, V. Saile, G. von Freymann, S. Linden, M. Wegener. *Science* **2009**, *325*, 1513.

[18] X. W. Gu, J. R. Greer. *Extreme Mech. Lett.* **2015**, *2*, 7.

[19] M. A. Zeeshan, R. Grisch, E. Pellicer, K. M. Sivaraman, K. E. Peyer, J. Sort, B. Özkale, M. S.

Sakar, B. J. Nelson, S. Pané. *Small* **2014**, *10*, 1284.

[20] G. Williams, M. Hunt, B. Boehm, A. May, M. Taverne, D. Ho, S. Giblin, D. Read, J. Rarity, R. Allenspach, S. Ladak. *Nano Res.* **2018**, *11*, 845.

[21] W. Zhou, S. M. Kuebler, K. L. Braun, T. Yu, J. K. Cammack, C. K. Ober, J. W. Perry, S. R. Marder. *Science* **2002**, *296*, 1106.

[22] I. Bernardeschi, O. Tricinci, V. Mattoli, C. Filippeschi, B. Mazzolai, L. Beccai. *ACS Appl. Mater. Interfaces* **2016**, *8*, 25019.

[23] A. Braun, S. A. Maier. *ACS Sens.* **2016**, *1*, 1155.

[24] E. H. Waller, G. von Freymann. *Nanophotonics* **2018**, *7*, 1259.

[25] L. Hirt, A. Reiser, R. Spolenak, T. Zambelli. *Adv. Mater.* **2017**, *29*, 1604211.

[26] J. Serbin, A. Egbert, A. Ostendorf, B. N. Chichkov, R. Houbertz, G. Domann, J. Schulz, C. Cronauer, L. Fröhlich, M. Popall. *Opt. Lett.* **2003**, *28*, 301.

[27] X. Zhou, Y. Hou, J. Lin. *AIP Adv.* **2015**, *5*, 030701.

[28] T. Tanaka, H.-B. Sun, S. Kawata. *Appl. Phys. Lett.* **2002**, *80*, 312.

[29] W. H. Teh, U. Dürig, U. Drechsler, C. G. Smith, H.-J. Güntherodt. *J. Appl. Phys.* **2005**, *97*, 054907.

[30] H.-Z. Cao, M.-L. Zheng, X.-Z. Dong, F. Jin, Z.-S. Zhao, X.-M. Duan. *Appl. Phys. Lett.* **2013**, *102*, 201108.

[31] T. Bückmann, R. Schittny, M. Thiel, M. Kadic, G. W. Milton, M. Wegener. *New J. Phys.* **2014**, *16*, 033032.

[32] K. A. Cooper, C. Hamel, B. Whitney, K. Weilermann, K. J. Kramer, Y. Zhao, H. Gentile. *Conformal photoresist coatings for high aspect ratio features.* SUSS MicroTec Waterbury Center, VT, USA, **2007**.

[33] S. M. George. *Chem. Rev.* **2010**, *110* 111.

Table I. Angles with respect to surface normal and thicknesses d used in the multiple angle evaporation sequence.

Angle (°)	d **Ti** (nm)	d **Au** (nm)
± 75	1	3
± 60	2	5
± 45	3	10
± 30	3	10
± 15	4	15
0	6	30

Table of contents: Direct laser writing is demonstrated to be well suited for fabricating nano- to microscale metallic structures using lift-off and a positive-tone photoresist on flat substrates, and uniquely, also on uneven substrates with elevation changes as high as 20 μm. Such fabrication is practically impossible with more standard lithographic techniques. An expression for how the line width varies with the scanning speed is also derived.

Keyword: Direct laser writing

Samuli Heiskanen, Zhuoran Geng, Jaakko Mastomäki, Ilari J. Maasilta*

Nanofabrication on Two- and Three-dimensional Topography via Positive-tone Direct-write Laser Lithography

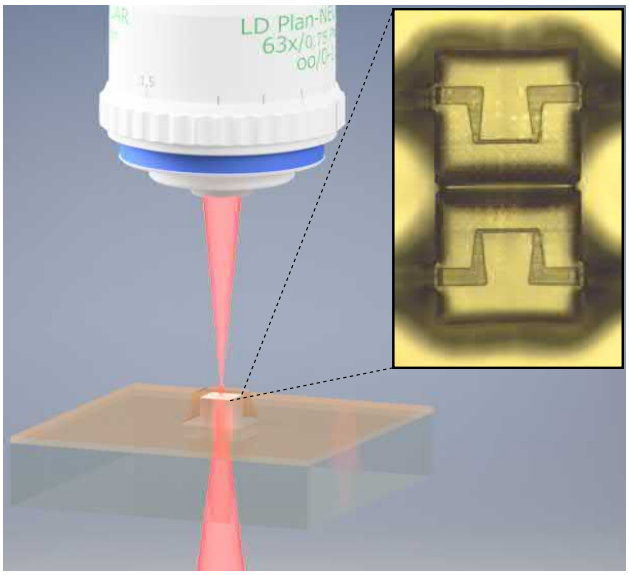

Figure 8. ToC figure

Supporting Information

Nanofabrication on Two- and Three-dimensional Topography via Positive-tone Direct-write Laser Lithography

*Samuli Heiskanen, Zhuoran Geng, Jaakko Mastomäki, Ilari J. Maasilta**

DERIVATION OF THE LINE WIDTH OF TWO-PHOTON DIRECT LASER WRITING

Here, we derive the equation for the line width of two-photon absorption (TPA) based direct laser writing (DLW), if the sample is in linear, continuous motion, Eq. (1) of the main article. The starting point is the rate equation [1, 2] for the position and time dependent density of radicals in the photoresist, $\rho(\mathbf{r}, t)$:

$$\frac{\partial \rho(\mathbf{r}, t)}{\partial t} = [\rho_0 - \rho(\mathbf{r}, t)]\sigma_2 I^2(\mathbf{r}, t), \tag{1}$$

with ρ_0 the primary initiator particle density of the resist, σ_2 is the effective two-photon cross-section for the generation of radicals [1], and $I(\mathbf{r}, t)$ the position and time dependent photon flux intensity (photons/area/s).

In literature, [1, 2], Eq. (1) was solved for the stationary stage case, and assuming that the radicals do not decay or diffuse within the time scales studied. With those assumptions, it is possible to disregard the inherent time dependence of the intensity I due to the pulsed nature of the laser, and only work with the time averaged, constant intensity $\tilde{I}(\mathbf{r}) = \int_T dt I(\mathbf{r}, t)/T$, where T refers to the period of the pulses (inverse of repetition rate). In other words, we are interested in the dynamics only at time scales much longer than T. In our DLW setup, the repetition rate of the laser is 80 MHz, giving $T = 12.5$ ns. With such assumptions, Eq. (1) can trivially be solved, with the result [1, 2]

$$\rho(\mathbf{r}, t) = \rho_0(1 - e^{-\sigma_2 \tilde{I}^2(\mathbf{r})t}). \tag{2}$$

Here, we extend the discussion to a moving stage, giving another slow time dependence that cannot be integrated out. At this point we assume a Gaussian spatial beam intensity

profile, which is not a rigorously correct at the laser focal plane [3], but a very good approximation, as we are not interested in the tails of the profile. Thus, if we consider only the focal plane and denote the beam waist there ω_0, the short-time averaged Gaussian beam can be written $\tilde{I}(\mathbf{r}) = I_0 \exp(-2|\mathbf{r} - \mathbf{r}_0(t)|^2/\omega_0^2)$, where $\mathbf{r}$ is now a two-dimensional vector in the focal plane, and $\mathbf{r}_0(t)$ the center of the beam, which is moving with respect to the stage, and is thus time dependent. If we discuss linear, constant velocity motion and fix the coordinates in such a way that the beam moves in the direction of the x-coordinate with velocity v, we obtain $|\mathbf{r}-\mathbf{r}_0(t)|^2 = (x-vt)^2+y^2$, and can write for the square of the intensity

$$\tilde{I}^2(x,y,t) = I_0^2 e^{-4y^2/\omega_0^2} e^{-4(x-vt)^2/\omega_0^2} = f(y)g(x,t), \tag{3}$$

where the last line defines the notation for the following discussion, i.e. $f(y) = I_0^2 \exp(-4y^2/\omega_0^2)$, $g(x,t) = \exp[-4(x-vt)^2/\omega_0^2]$. Now we can look back at Eq. (1), and rewrite it with our new notation as

$$\frac{\partial \rho(x,y,t)}{\partial t} = [\rho_0 - \rho(x,y,t)]\sigma_2 f(y) g(x,t), \tag{4}$$

which is a first-order non-homogeneous linear equation for ρ, and thus can be solved exactly [4]. Eq. (4) simplifies with the notation $\rho' = \rho - \rho_0$, in which case it reads $\partial\rho'/\partial t = -\rho'\sigma_2 f(y) g(x,t)$, which can be solved to give $\rho' = A\exp(-\int dt \sigma_2 f(y) g(x,t))$. Thus, we need to find the time integral of $g(x,t)$, which gives

$$\int g(x,t)dt = \int e^{-4(x-vt)^2/\omega_0^2} dt = \frac{\sqrt{\pi}}{4}\frac{\omega_0}{v}\ \mathrm{erf}\left(\frac{2(vt-x)}{\omega_0}\right),$$

with $\mathrm{erf}(x)$ the error function. Therefore, we can write for ρ the general solution

$$\rho(x,y,t) = \rho_0 + A e^{-\sigma_2 f(y)\frac{\sqrt{\pi}}{4}\frac{\omega_0}{v}\mathrm{erf}\left(\frac{2(vt-x)}{\omega_0}\right)}. \tag{5}$$

The initial condition will be set at $t = -\infty$ when the laser beam center is far away at $x = -\infty$ and no radicals yet exist, i.e. $\rho = 0$. That condition gives $\rho_0 + A\exp\left(+\sigma_2 f(y)\frac{\sqrt{\pi}}{4}\frac{\omega_0}{v}\right) = 0$, where the + sign appears because $\mathrm{erf}(x) \to -1$ as $x \to -\infty$. Thus, we get $A = -\rho_0 \exp\left(-\sigma_2 f(y)\frac{\sqrt{\pi}}{4}\frac{\omega_0}{v}\right)$, and substituting that into Eq. (5), we finally obtain the solution

$$\rho(x,y,t) = \rho_0 \left\{1 - e^{-\sigma_2 f(y)\frac{\sqrt{\pi}}{4}\frac{\omega_0}{v}\left[1+\mathrm{erf}\left(\frac{2(vt-x)}{\omega_0}\right)\right]}\right\}. \tag{6}$$

We plot this function vs. x at several different time points in Fig. 1, and see that it forms a step-like feature, which moves from left to right with velocity v as time passes. The

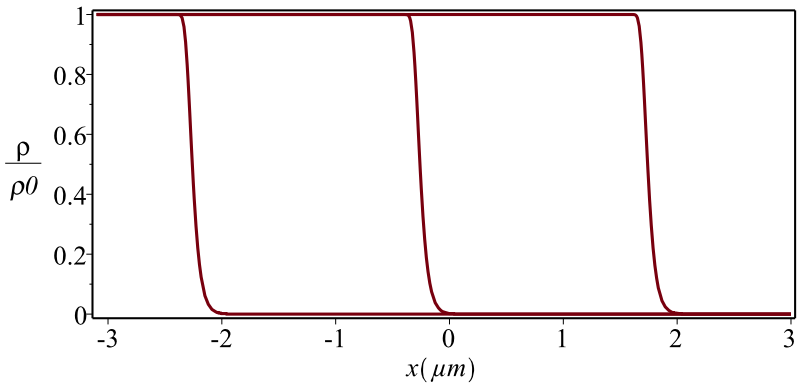

FIG. 1. Examples of the radical density profile functions of a beam moving in x-direction, Eq. (6), at different times.

density of radicals left behind the moving beam depends on σ_2 (the resist), I_0 (the laser power), and the ratio of beam waist to velocity ω_0/v.

With the solved radical profile ρ, we are in a position to derive the developed line width in y-direction. As in the literature for a stationary beam [1, 2], the width is defined as the region where the radical density is above some threshold level ρ_{th}, $\rho(x, y, t) \geq \rho_{th}$. Using the explicit expression for $f(y) = I_0^2 e^{-4y^2/\omega_0^2}$ we arrive at a condition

$$y^2 \leq \frac{\omega_0^2}{4} \ln \left\{ \frac{\sigma_2 I_0^2}{C} \frac{\sqrt{\pi}}{4} \frac{\omega_0}{v} \left[1 + \mathrm{erf}\left(\frac{2(vt - x)}{\omega_0} \right) \right] \right\}, \tag{7}$$

where we have defined $C = \ln[\rho_0/(\rho_0 - \rho_{th})]$. As we are interested only in the limit when the beam has passed the regions of interest in x, we can look at the $t \to \infty$ limit, in which case $\mathrm{erf}(x) \to 1$. Then we take the square root of Eq. (7) and multiply it by two to obtain the final expression for the line width $w = 2|y|$:

$$w = \omega_0 \sqrt{\ln\left(\frac{\sigma_2 I_0^2}{C} \frac{\sqrt{\pi}}{2} \frac{\omega_0}{v} \right)}, \tag{8}$$

the expression given in the main text.

[1] J. Serbin, A. Egbert, A. Ostendorf, B. N. Chichkov, R. Houbertz, G. Domann, J. Schulz, C. Cronauer, L. Fröhlich, and M. Popall, Opt. Lett. **28**, 301 (2003).

[2] X. Zhou, Y. Hou, and J. Lin, AIP Advances **5**, 030701 (2015).

[3] L. Novotny and B. Hecht, *Principles of Nano-Optics* (Cambridge University Press, 2006).

[4] H. J. W. G. B. Arfken and F. E. Harris, *Mathematical Methods for Physicists, 7th Ed.* (Elsevier, 2013).